# The Gut Metagenome Changes in Parallel to Waist Circumference, Brain Iron Deposition, and Cognitive Function

Gerard Blasco,[1,2] José Maria Moreno-Navarrete,[3,4] Mireia Rivero,[5] Vicente Pérez-Brocal,[6,7,8] Josep Garre-Olmo,[9] Josep Puig,[1,2] Pepus Daunis-i-Estadella,[10] Carles Biarnés,[2] Jordi Gich,[4] Fernando Fernández-Aranda,[11] Ángel Alberich-Bayarri,[12] Andrés Moya,[6,7,8] Salvador Pedraza,[2] Wifredo Ricart,[3,4] Miguel López,[13,14] Manuel Portero-Otin,[15] and José-Manuel Fernandez-Real[3,4]

[1]Research Unit, Institute of Diagnostic Imaging (IDI), Parc Sanitari Pere Virgili, Barcelona 08023, Spain; [2]Medical Imaging, Girona Biomedical Research Institute (IDIBGI), Hospital Universitari Dr Josep Trueta, Girona 17007, Spain; [3]Department of Diabetes, Endocrinology and Nutrition (UDEN), Girona Biomedical Research Institute (IDIBGI), CIBER de la Fisiopatología de la Obesidad y la Nutrición (CIBERobn, CB06/03/0010), Instituto de Salud Carlos III (ISCIII), Girona 17007, Spain; [4]Department of Medicine, University of Girona, Girona 17007, Spain; [5]Neurology Department, Girona Biomedical Research Institute (IDIBGI), Hospital Universitari Dr Josep Trueta. Girona 17007, Spain; [6]Genomics and Health Area of the Fundación para el Fomento de la Investigación Sanitaria y Biomédica de la Comunidad Valenciana (FISABIO)-Salud Pública, Valencia 46020, Spain; [7]Institut Cavanilles de Biodiversitat i Biologia Evolutiva, Universitat de València, Valencia 46980, Spain; [8]CIBER Epidemiología y Salud Pública (CIBERESP), Madrid 28029, Spain; [9]Research Group on Aging, Disability and Health, Girona Biomedical Research Institute (IDIBGI), Girona 17007, Spain; [10]Department of Computer Science, Applied Mathematics, and Statistics, University of Girona. Girona 17004, Spain; [11]Department of Psychiatry, University Hospital of Bellvitge, Bellvitge Biomedical ResearchInstitute (IDIBELL), CIBER Fisiopatología Obesidad y Nutrición (CIBERObn), Instituto Salud Carlos III, Barcelona 08908, Spain; [12]Biomedical Imaging Research Group (GIBI230), QUantitative Imaging Biomarkers In Medicine (QUIBIM SL), La Fe Polytechnics and University Hospital, La Fe Health ResearchInstitute, Valencia 46026, Spain; [13]NeurObesity Group; Department of Physiology, Center for Research in Molecular Medicine and Chronic Diseases (CiMUS), University of Santiago de Compostela-Instituto de Investigación Sanitaria, Santiago de Compostela 15782, Spain; [14]CIBERObn, Santiago de Compostela 15706, Spain; and [15]Nutren Group, Department of Experimental Medicine, Lleida Biomedical Research Institute (IRBLleida) and Agroalimentary Science and Technology Park (PCiTAL)–University of Lleida, Lleida 25003, Spain

**Context:** Microbiota perturbations seem to exert modulatory effects on emotional behavior, stress-, and pain-modulation systems in adult animals; however, limited information is available in humans.

**Objective:** To study potential relationships among the gut metagenome, brain microstructure, and cognitive performance in middle-aged, apparently healthy, obese and nonobese subjects after weight changes.

**Design:** This is a longitudinal study over a 2-year period.

**Setting:** A tertiary public hospital.

**Patients or Other Participants:** Thirty-five (18 obese) apparently healthy subjects.

**Intervention(s):** Diet counseling was provided to all subjects. Obese subjects were followed every 6 months.

**Main Outcome Measure(s):** Brain relaxometry (using magnetic resonance R2*), cognitive performance (by means of cognitive tests), and gut microbiome composition (shotgun).

ISSN Print 0021-972X ISSN Online 1945-7197
Printed in USA

Received 14 January 2017. Accepted 30 May 2017.
First Published Online 7 June 2017

Abbreviations: BMI, body mass index; HIC, hepatic iron concentration; MR, magnetic resonance; RA, relative abundance; ROCFT, Rey–Osterrieth Complex Figure Test; TE, echo time; TMT, Trail Making Test; TR, repetition time; VF, verbal fluency.

**Results:** R2* increased in both obese and nonobese subjects, independent of weight variations. Changes in waist circumference, but not in body mass index, were associated with brain iron deposition (R2*) in the striatum, amygdala, and hippocampus in parallel to visual-spatial constructional ability and circulating beta amyloid A$\beta$42 levels. These changes were linked to shifts in gut microbiome in which the relative abundance of bacteria belonging to Caldiserica and Thermodesulfobacteria phyla were reciprocally associated with raised R2* in different brain nuclei. Of note, the increase in bacteria belonging to Tenericutes phylum was parallel to decreased R2* gain in the striatum, serum A$\beta$42 levels, and spared visual-spatial constructional ability. Interestingly, metagenome functions associated with circulating and brain iron stores are involved in bacterial generation of siderophores.

**Conclusions:** Changes in the gut metagenome are associated longitudinally with cognitive function and brain iron deposition. (***J Clin Endocrinol Metab*** **102: 2962–2973, 2017)**



Recent advances in research have described the potential role of gut microbiome on broad aspects of human health, including emotional behavior and cognition through the gut-brain axis (1, 2). Perturbations in the gut microbiome have been implicated in the development of obesity and related complications (3). Obesity and weight variations have been associated with altered representation of bacterial genes, reduced bacterial diversity, and changes in the relative abundance (RA) of the two dominant phyla, the Bacteroidetes and the Firmicutes (4). In particular, an elevated ratio of Firmicutes to Bacteroidetes (increases in members of the phylum Firmicutes or decreases in the phylum Bacteroidetes) has been found in subjects with obesity, whereas a decrease in this ratio has been found in relation to weight loss (5, 6). Increased gut microbiome diversity also correlates with lower weight gain in humans, independent of calorie intake and other confounders (7).

Crosstalk among the gastrointestinal tract, gut microbiome, and central nervous system has been implicated in the regulation of gut function in both healthy and diseased states (1, 2). Alterations in gut microbiome could affect human brain health by producing systemic and/or central nervous system inflammation, stimulate dysfunctional responses of the adaptive immune system, exert neurotoxicity, and/or stimulate afferent neurons of the enteric nervous system (1). Through these underlying mechanisms, preclinical evidence indicates the potential relationship between the gut microbiome and hypothalamic-pituitary axis involving alterations in emotional behavior, anxiety, depression, stress response, and working memory (2, 8).

However, in contrast to the strong preclinical evidence, there is only suggestive evidence that a similar relationship might exist in humans (8). A preliminary study found an association among bacterial diversity (Shannon diversity index); the RA of bacteria belonging to Actinobacteria phylum; microstructural changes at the hypothalamus, caudate nuclei, hippocampus, thalamus, and amygdala; and worse cognitive test scores related to speed and attention (9). On the other hand, the intake of probiotics containing Bifidobacterium, *Streptococcus*, *Lactobacillus*, and Lactococcus induced changes in the brain response to an emotional faces attention task and beneficial effects on anxiety- and depression-related behaviors (10).

Magnetic resonance (MR) has been widely used for noninvasive assessment of structural, metabolic, and functional brain changes in apparently healthy subjects. MR relaxation rates of R2*, based on the contribution of paramagnetic ferritin-loaded cells to the T2* relaxation signal, is a well-established method for brain iron assessment (11). In animal models and in humans, increased brain iron load at the basal ganglia, amygdala, and hippocampus has been associated with worse cognitive performance, executive functions, and verbal working memory scores (12–14). Of note, basal ganglia are involved in emotional, associative, motivational, and cognitive functions, whereas the thalamus and striatum are mainly implicated in sensory and motor mechanisms, including response selection and initiation (15). More recently, increased brain iron load by means of relaxation rates of R2* was found to be linked to worse cognitive test scores related to motor speed, attention, and memory in subjects with obesity (9).

We hypothesized that changes in brain structure and cognitive function are associated with shifts in gut microbiome in middle-aged subjects. Accordingly, we aimed to examine gut microbiome, brain microstructure by means of R2* values, and validated neurocognitive test in middle-aged lean and obese subjects over a 2-year period in which the obese subjects were encouraged to lose weight.

## Materials and Methods

### Study design

From January to September 2012, we undertook a cross-sectional, case-control study-based MR iron assessment in

25 middle-aged subjects with obesity [body mass index (BMI) >30 kg/m$^2$; age range, 30 to 65 years] in whom type 2 diabetes and transferrin saturation >45% were specifically excluded. Nineteen healthy subjects without obesity (BMI <30 kg/m$^2$) were matched for sex and age and served as the control group. All subjects reported stable weight during the preceding 3 months. In that cross-sectional study, exclusion criteria for both groups were any manifestation of cardiovascular disease, systemic disease, infection in the previous month, serious chronic illness, >20 g ethanol intake per day, use of medications that might interfere with insulin action, and inability to understand study procedures. After the procedure, subjects with obesity were instructed to maintain a reduction in daily caloric intake of 500 to 800 kcal during the study period. A hypocaloric diet containing 25 or 20 kcal/kg was recommended. The composition of the diet was 15% proteins, 30% fat (<10% saturated fat), 55% carbohydrates, and 20 to 25 g dietary fiber. As a limitation, diet information was not collected in these subjects.

Longitudinal study was performed from October 2014 to January 2015 in those subjects who agreed to undertake follow-up MR examinations and provide specific written informed consent. Thus, in this study, 35 volunteers (17 subjects with obesity and 18 control subjects) were included.

The institutional review board, the Ethics Committee and the Committee for Clinical Research at the University Hospital of Girona Dr. Josep Trueta (Girona, Spain), approved the study protocol, which certifies that all applicable rules for the ethical use institutional information and samples from human volunteers were followed during this research. All procedures were in accordance with the ethical standards of the responsible committee on human experimentation (institutional and national) and with the Helsinki Declaration of 1975, as revised in 2008. All participants provided their written informed consent before the start of this study.

## Anthropometry and laboratory measurements

Patients underwent anthropometric measurements, and, after 8 hours' fasting, provided blood for measurement of plasma lipids, glucose, and insulin. Glucose and lipid levels were determined by standard laboratory methods. Serum insulin was measured by radioimmunoassay. Plasma $\beta$-amyloid$_{(1\text{-}42)}$ concentration was included as a variable considering the previous reported relationship among MR brain relaxometry signal, iron, and $\beta$-amyloid in a context of increased risk for Alzheimer's disease or $\beta$-amyloid plaque (16). Plasma $\beta$-amyloid$_{(1\text{-}42)}$ concentration was measured using INNOTEST $\beta$-amyloid$_{(1\text{-}42)}$ enzyme-linked immunoassay absorbance kit (Ref81587, Fujirebio Europe N.V., Belgium) according to the manufacturer's protocol, with intra- and interassay coefficients of variation <10%. The percent change in anthropometric and analytical parameters between baseline and follow-up were calculated as (follow-up – baseline)/baseline × 100.

## MR imaging acquisition and image preprocessing

All subjects were studied on a 1.5T Gyroscan Intera system (Philips Health Care, Best, The Netherlands) with an eight-channel head coil. As a part of a larger study protocol, a multislice fluid attenuation inversion recovery (T2 fluid attenuated inversion recovery) with repetition time (TR) /echo time (TE)/inversion time = 6500/120/2200 ms, 90° flip angle, 0.78 × 0.78 in-plane resolution, slice thickness 5 mm without gap, and 20 axial slices was used to exclude preexisting brain lesions. Brain iron was assessed using a multiecho gradient echo sequence with TR/first ET/Δ = 800/2.2/5 ms, 80° flip angle, 2 × 2 in-plane resolution, slice thickness 5 mm without gap, and 20 axial slices. After acquisition, T2* and R2* maps were computed in Olea Sphere 3.0 (Olea Medical, La Ciotat, France) using Bayesian analysis algorithm, where R2* maps were calculated as R2* = 1/T2* and T2* maps were calculated by fitting the signal decay curve of the respective magnitude multiecho data. In addition, a brain extraction tool was used to delete all nonbrain tissues of calculated T2* and R2* maps. R2* were measured in seconds$^{-1}$. There are well-established methods to convert liver MR signal intensities into values of iron expressed in micromoles per gram (17, 18). However, to our knowledge, there are not any established method to convert T2* signal intensity decay into micromoles per gram of iron in brain. Thus, we choose not convert the brain R2* values into micromoles per gram of iron. Previous studies showed positive associations between hepatic iron concentrations (HICs) and brain iron load by means of MR signal in middle-aged subjects with obesity (14). Thus, HIC was assessed using signal intensity ratio from a single slice T2* and proton density acquisitions (TR = 140 ms; TE = 14 ms and TR = 140 ms; TE = 4 ms, respectively). The averages of the measurements of liver and muscle signal intensities were used to estimate the hepatic iron.

## Image analysis

All calculated maps were analyzed using SPM8 (Welcome Department of Imaging Neuroscience, Institute of Neurology, London, UK) running MATLAB 7.7 (The MathWorks, Natick, MA) on a Windows 7 computer. The image postprocessing involves two steps. First, to improve the image normalization process in the study population, an R2* template was generated. To create the template, T2* and R2* maps from 18 healthy control subjects at baseline were coregistered by nonrigid methods. After, T2* images were spatially normalized to a standard EPI template using a 1 × 1 × 1 spatial resolution; deformation parameters were applied to corresponding R2* images. The average of normalized R2* maps were used to create the template. In a second step, baseline and follow-up R2* maps from all subjects were normalized to the R2* template and the resulting images were spatially smoothed using spatially stationary Gaussian filter with a kernel width of 6 mm.

The brain regions of interest were selected based on previous meta-analyses and cross-sectional and longitudinal evidence showing increased iron load at the amygdala, hippocampus, caudate, putamen, pallidum, and thalamus in apparently healthy subjects in association with executive function and verbal working memory scores (12, 14, 19). Jülich's Histological Atlas and Harvard-Oxford Subcortical Atlas were used to obtain R2* values at these regions. If necessary, the regions of interest were manually adjusted for each subject using MRIcro (www.mricro.com) to ensure that no cerebrospinal fluid or white matter was included. The percent of change between R2* images at baseline and follow-up [(R2*follow-up – R2*baseline)/R2*baseline × 100] were calculated for all subjects with longitudinal MR examination (n = 35). Voxelwise nonparametric permutation inference with 5000 randomized iterations (FSL, Oxford Centre for Functional MRI of the Brain, Oxford, UK) were used to evaluate the association of age and

obesity variations with R2* rates changes in the 35 subjects with MR examination. The same statistical approach was used to assess the relationship between gut microbiome and R2* rates changes in the 27 subjects who agreed to perform the gut metagenomic analysis. Statistically significant increases or decreases in R2* change were detected at an individual voxel threshold of $P < 0.001$.

## Gut metagenome analyses

Eight of the 35 patients included in this longitudinal study did not provide feces samples at follow-up; thus, 27 subjects (14 subjects with obesity and 13 control subjects) were included in the gut microbiome analyses. Total DNA was extracted from frozen human stools using the QIAamp DNA mini stool kit (Qiagen, Courtaboeuf, France). Quality was assessed with the prinseq-lite program (20), applying the following parameters: min_length: 50; trim_qual_right: 20; trim_qual_type: mean; and trim_qual_window: 20. R1 and R2 from Illumina sequencing were joined using *fastq-join* from the ea-tools suite. Three files per sample were obtained, one of joined pairs of reads and two of not joined reads. The fastq files were converted into fasta files using the "fastq_to_fasta" tool from the FastX-Toolkit program. Those files were filtered from human contamination using the bowtie2 program (21) against the human genome, downloaded from the National Center for Biotechnology Information (NCBI) FTP site (ftp://ftp.ncbi.nlm.nih.gov/genomes/H_sapiens/). The unaligned files (*i.e.*, those that did not map against the human genome) were the input files of a BLASTn search against a customized bacterial database (Bacteria_2015_06_09) consisting of the Human Microbiome and the bacterial genomes downloaded from the NCBI FTP site (ftp://ftp.ncbi.nlm.nih.gov/genomes/humanmicrobiom/Bacteria/ and ftp://ftp.ncbi.nlm.nih.gov/genomes/archive/old_refseq/Bacteria/) updated to July 2014 and June 2015, respectively. The best hits of the BLASTn output files were extracted, converted into contingency tables, and transformed into the BIOM format to be used as input files of the Quantitative Insights Into Microbial Ecology open-source software pipeline, version 1.9.0, which implemented the RA calculations of the bacterial hits at different taxonomical levels. This pipeline was also used to estimate the alpha diversity or diversity within samples through the calculation of the Shannon diversity index of the samples, using the following parameters for rarefactions: 20 steps of 40 iterations each, comprising between 100 and 213,096 reads (the number of reads of the smallest sample) with increments of 10,654 reads per step. Diversity was calculated for the first and second visits of the subjects. Beta diversity or diversity among samples was also estimated to generate principal coordinates analysis of the samples from Bray-Curtis dissimilarity and Canberra distance matrices. Detailed information related to the metagenomic approach is included in the Supplemental Methods.

## Neuropsychological assessment

The neuropsychological examination was carried out by experienced neuropsychologists. The neuropsychological examination was based on tasks that required mainly an involvement of the frontal lobe. The prefrontal cortex participates in the organization of goal-directed behaviors, and is one of the first regions to structurally decline during the aging process. This selection was based on the hypothesis that cognitive performance of frontal-related tasks in middle-aged adults would be more sensitive to negative effects. The length of a cognitive examination can produce a progressive decrease in the cognitive abilities to execute the tasks (resulting from fatigue). To standardize the neuropsychological examination and to avoid sources of measurement error, we decided to administer all the neuropsychological battery in the same order. The neuropsychological assessment administration time was about 35 to 45 minutes depending on the patient. Immediate and delayed visual memories were assessed with the Rey–Osterrieth Complex Figure Test (ROCFT) and executive functioning was evaluated with the Trail Making Test (TMT) and the phonemic and semantic verbal fluency (VF) tasks. The ROCFT assesses several cognitive functions such as visual-spatial constructional ability, visual memory (immediate and delayed), motor function, and components of executive function (planning and working memory). The material consists of a sheet with the stimuli figure. The participants were asked to copy the figure as accurately as possible. Three minutes following the completion of the copy, to assess immediate recall, subjects were asked to draw the figure from memory, as accurately as possible and with no time limit. Finally, 20 minutes following completion of the immediate recall, subjects were asked to draw the figure from memory again to assess delayed recall. According to the scoring system of the ROCFT, the 18 elements of the figure are scored based on distortion and placement. The quantitative evaluation is scored out of a maximum of 36 points. The TMT is a measure of attention, speed, and mental flexibility. The TMT consists of two parts (TMT-A and TMT-B). The TMT-A consists of a standardized page on which the numbers 1 to 25 are scattered within circles; the participants were asked to connect the numbers in order as quickly as possible. Similarly, the TMT-B consists of a standardized page that included the numbers 1 to 13 and the letters A to L. The participants were instructed to draw lines connecting numbers and letters in order, alternating numbers and letters. Before starting the test, a practice trial of six items was administered to the participants to make sure that they understood both tasks. When a participant made an error during the test performance, the examiner pointed it out and explained it, then guided the participant to the last circle completed correctly, and requested the participant to continue with the task. A maximum time of 300 seconds was allowed before discontinuing the test. Direct scores of TMT were the time in seconds taken to complete each task (A and B). The VF is a measure of executive functioning. The participants were asked to say words beginning with the letter "P", and to say words pertaining to the "animals" category. They had to do the test as quickly as possible; the number of words produced during 1 minute was scored for both phonemic and semantic VF.

## Statistical analysis

Results are expressed as medians and quartiles for continuous variables and as frequencies for categorical variables. We used nonparametric statistical analyses considering nonnormal distribution of the variables because of the relative small sample size the study. The Mann-Whitney *U* test was used to determine differences between the study groups (subjects with and without obesity); the Wilcoxon test was used to determine longitudinal intrasubject differences. The correlation between the percentages of change for the quantitative variables was assessed using Spearman rho analysis. Those variables associated with the percent of R2* change ($P < 0.05$) were included in the voxelwise

nonparametric permutation inference. Clustering analyses was included to graphically determine the relationship between changes in microbiome, R2* values, and phenotype variations. We used multivariate linear regression analyses to assess the associations between variations changes in microbiome and R2* values adjusting for age, sex, and/or waist circumference. For clustering analyses and graphic representation, variables were analyzed by using the hclust, plot, and clustsig R package. Other statistical analyses were performed with R package and SPSS, version 19 (SPSS, Inc., Chicago, IL).

## Results

Results of the longitudinal differences in gut microbiome, MR relaxometry, and cognitive function among subjects with and without obesity are shown in Table 1. Over a 2-year period, BMI was decreased in subjects with obesity, whereas control subjects increased in waist circumference. MR relaxometry R2*, a parameter that indicates iron content, but also $\beta$-Amyloid deposition (16), increased mainly at the pallidum, putamen, thalamus, and hippocampus in both groups. The degree of increase in relaxometry in the striatum was not significantly different between lean and obese subjects. Figure 1 shows the regions where the increase in R2* was more marked in the voxelwise analysis after 5000 iterations ($P < 0.001$). Of note, the 2-year related raise was observed in all subjects, including those that gained or lost weight during this period, indicating that this process was independent of BMI. However, despite BMI not being linked to changes in R2*, the percent change in waist circumference was positively associated with R2* increase in the striatum and other brain nuclei (amygdala, hippocampus). A trend was observed with worsening of visual-spatial constructional ability (Fig. 2). Interestingly, the increase in circulating $\beta$-amyloid A$\beta$42 levels was positively associated with the change in visual-spatial constructional ability and immediate memory and negatively with the increase in R2* (Fig. 2), with the former in line with other longitudinal studies (22). This could seem counterintuitive but a decrease in A$\beta$42 levels are thought to reflect compartmentalization of A$\beta$ peptides in the brain and have been related to the development of Alzheimer's disease (22). Copy memory scores were inversely associated with R2* at the left caudate ($r = -0.409$; $P = 0.034$), left and right pallidum ($r = -0.383$; $P = 0.048$ and $r = -0.524$; $P = 0.005$, respectively), and right putamen ($r = -0.575$; $P = 0.002$). Immediate and deferred memory scores were inversely associated with R2* at the right thalamus ($r = -0.403$; $P = 0.037$ and $r = -0.395$; $P = 0.041$). Worse TMT-A scores were associated with increased R2* at the right and left pallidum ($r = 0.440$; $P = 0.024$ and $r = 0.529$; $P = 0.005$).

Fasting glucose, glycated hemoglobin, and low high-density lipoprotein cholesterol levels improved at follow-up after dietary recommendations in subjects with obesity. HIC was reduced significantly within subjects with obesity but remained higher than in the control group. The percent change in BMI was positively correlated with the RA of bacteria belonging to Caldiserica phylum ($r = 0.602$; $P = 0.029$) in the control group and negatively correlated with Armatimonadetes ($r = -0.78$; $P = 0.004$) and Synergistetes ($r = -0.60$; $P < 0.023$) in subjects with obesity at baseline.

HIC was higher in those subjects with obesity at baseline ($P < 0.001$) and follow-up ($P = 0.007$) and associated with increased R2* at left amygdala ($r = 0.346$; $P = 0.043$), caudate ($r = 0.501$; $P = 0.002$), pallidum ($r = 0.380$; $P = 0.024$), and putamen ($r = 0.447$; $P = 0.007$) at baseline. HIC was inversely associated with Bacteroidetes at follow-up ($r = -0.559$; $P = 0.002$). The percent of HIC change was positively correlated with the percent of change in BMI ($r = 0.355$; $P = 0.036$), Actinobacteria ($r = 0.407$; $P = 0.039$), and Cloacimonetes ($r = 0.599$; $P = 0.004$), but no association with brain R2* changes was found. The RA of Prevotellaceae correlated positively with BMI ($r = 0.34$; $P = 0.031$), whereas the RA of Bacteroidaceae ($r = -0.34$; $P = 0.03$), Rikenellaceae ($r = -0.46$; $P = 0.002$), and Lachnospiraceae ($r = -0.35$; $P = 0.02$) was negatively correlated.

We also observed changes when subjects were classified according to weight loss versus weight gain, independent of being obese or not (Supplemental Table 1). Of note, gut microbiome composition interacted with these relationships. Clustering analyses showed that changes in specific gut microbiota bundled together with neuroimaging R2* values (Fig. 3). For instance, the percent of change in RA of Gemmatimonadetes, Bacteroidetes, and Proteobacteria run in parallel with 2-year differences in R2* at the caudate nuclei. We then explored the change in RA of the different phyla. On univariate analyses, the percent of change in bacteria belonging to Caldiserica phylum was positively associated, whereas the percent of change in Candidatus Saccharibacteria, Tenericutes, and Thermodesulfobacteria RA was negatively associated with the percent change of R2* increase (Fig. 2). In multivariate regression analyses, the surge in Chlorobi RA was positively associated with the increase in R2* in left superficial amygdala and right hippocampus [Fig. 4(a)]. In this last territory, the phyla Fibrobacteres, Synergistetes, and Tenericutes RA were reciprocally associated with right hippocampus R2*. In the right caudate nucleus, the increase in R2* was more accentuated in young subjects (below the median age of the sample) and tended to be different in men and women ($P = 0.06$). After adjusting for age and sex, the increase in Chlorobi, Bacteroidetes, Proteobacteria, and Gemmatimonadetes RA was positively associated with the increase in R2* in the right caudate nucleus in parallel to a lower

**Table 1. Clinical Data, Neuropsychological Scores, and Brain Relaxometry R2*According to Study Groups at Baseline and 2-Year Follow-Up**

| Subjects Included in the MR Analysis | Control Group (n = 18) | | | Subjects With Obesity (n = 17) | | | Differences Between Study Groups | |
|---|---|---|---|---|---|---|---|---|
| | Baseline | Follow-Up | | Baseline | Follow-Up | | Baseline | Follow-Up |
| | Median (Q1–Q3) | Median (Q1–Q3) | *P* Value | Median (Q1–Q3) | Median (Q1–Q3) | *P* Value | *P* Value | *P* Value |
| Age, y | 50 (39–56.25) | 52 (42–59.5) | <0.000 | 53 (48–58) | 56 (51.5–60) | <0.000 | 0.203 | 0.186 |
| Sex, female frequency | 8 (—) | – (—) | — | 11 (—) | – (—) | — | 0,315 | — |
| Waist circumference, cm | 84 (74.25–91.5) | 90 (76–97) | 0.004 | 125.5 (122–134) | 114 (97.5–134) | 0.289 | 0.000 | <0.000 |
| BMI, kg/m$^2$ | 23.3 (21.6–25.82) | 23.9 (21.52–25.72) | 0.338 | 45.1 (39.1–47.45) | 36.5 (29.55–44.1) | 0.037 | 0.000 | <0.000 |
| Fasting glucose, mg/dL | 88 (83.5–96) | 96 (86.5–101) | 0.177 | 100 (92.5–103) | 90 (86.5–105) | 0.351 | 0.034 | 0.718 |
| Glycated hemoglobin, % | 5.45 (5.27–5.62) | 5.4 (5.1–5.5) | 0.004 | 5.8 (5.45–6.05) | 5.5 (5.2–5.8) | 0.063 | 0.020 | 0.066 |
| Triglycerides, mg/dL | 61 (43–99) | 62 (48.5–90) | 0.408 | 99 (68.5–150) | 96 (68.5–133) | 0.301 | 0.022 | 0.032 |
| LDL-cholesterol, mg/dL | 126 (91.75–143.25) | 114 (99–138.5) | 0.856 | 113 (100–148.5) | 98.5 (72–133) | 0.023 | 0.974 | 0.101 |
| HDL-cholesterol, mg/dL | 64 (51–77) | 66 (53.5–75) | 0.448 | 46 (43–54.5) | 56.5 (48.25–69.5) | 0.032 | 0.026 | 0.227 |
| Ferritin, ng/mL | 74 (38–125) | 80 (48–119) | 0.653 | 130 (74–222) | 123 (80–148) | 0.023 | 0.029 | 0.162 |
| Circulating $\beta$–amyloid, pg/mL | 33.57 (30.71–38.81) | 36.4 (29.18–42.41) | 0.463 | 36.04 (28.27–40.9) | 39.8 (35.04–42.87) | 0.140 | 0.856 | 0.317 |
| Copy memory score | 36 (34–36) | 36 (34–36) | 0.705 | 35 (33–36) | 36 (34–36) | 0.270 | 0.282 | 0.913 |
| Immediate memory score | 18 (15.87–24) | 23.25 (19.75–26) | 0.440 | 22 (13–27) | 23.75 (14.62–25.87) | 0.177 | 0.883 | 0.895 |
| Deferred memory score | 21 (13.5–24.87) | 25 (21.25–27) | 0.050 | 20 (11–28) | 23.75 (15.25–25.75) | 0.124 | 0.903 | 0.406 |
| Semantic fluency score | 21 (17–23.5) | 22.5 (18–24.75) | 0.326 | 19.5 (16–23.75) | 20 (18.5–24.5) | 0.197 | 0.532 | 0.588 |
| Phonemic fluency score | 31 (27.5–42) | 35 (28.25–43.25) | 0.091 | 27 (22.25–36.25) | 28 (21.5–36) | 1.000 | 0.246 | 0.063 |
| TMT-A, s | 27.5 (20.5–35.75) | 26 (24–33.75) | 0.507 | 50 (36.75–59.5) | 40 (29.5–48.5) | 0.090 | 0.001 | 0.015 |
| TMT-B, s | 87 (49–125) | 67.5 (45.75–100) | 0.086 | 105.5 (74–131.5) | 74.5 (58–103.75) | 0.013 | 0.622 | 0.509 |
| Hepatic iron, μmol Fe/g | 10.295 (8.54–11.79) | 9.82 (8.71–11.63) | 0.557 | 15.84 (14.33–18.3) | 12.79 (10.97–16.4) | 0.004 | 0.000 | 0.007 |
| Amygdala left R2* | 21.48 (20.45–23.02) | 23.72 (22.06–25.13) | 0.001 | 23.82 (21.64–25.77) | 24.57 (21.49–27.77) | 0.177 | 0.012 | 0.409 |
| Amygdala right R2* | 22.15 (20.66–22.97) | 24.53 (22.44–26.76) | 0.000 | 21.96 (18.85–24.68) | 23.38 (20.9–26.31) | 0.136 | 0.869 | 0.156 |
| Caudate left R2* | 14.51 (13.65–15.83) | 14.82 (13.48–15.71) | 0.327 | 14.92 (14.33–15.97) | 15.07 (14.05–15.66) | 0.795 | 0.210 | 0.621 |
| Caudate right R2* | 14.81 (13.21–15.73) | 15.22 (13.82–15.95) | 0.022 | 14.75 (13.84–15.59) | 15.7 (14.28–16.76) | 0.136 | 0.947 | 0.448 |
| Hippocampus left R2* | 20.62 (19.25–21.64) | 21.94 (20.91–22.49) | 0.006 | 20.05 (19.17–22.29) | 22.37 (20.97–23.89) | 0.006 | 0.921 | 0.322 |
| Hippocampus right R2* | 20.46 (19.92–21.71) | 21.96 (21.34–23.52) | 0.001 | 19.24 (17.99–21) | 20.78 (19.4–22.83) | 0.015 | 0.069 | 0.113 |
| Pallidum left R2* | 21.47 (20.52–22.17) | 21.97 (21.31–23.06) | 0.020 | 24.32 (22.73–25.36) | 25.51 (23.01–27.05) | 0.022 | 0.000 | <0.000 |
| Pallidum right R2* | 21.97 (20.97–22.78) | 23.33 (22.38–23.76) | 0.000 | 22.89 (21.14–24.54) | 24.97 (22.81–25.64) | 0.028 | 0.106 | 0.056 |
| Putamen left R2* | 18.51 (18.06–19.39) | 19.30 (18.94–19.85) | 0.002 | 20.41 (18.63–20.97) | 21.36 (19.7–22.55) | 0.017 | 0.008 | 0.001 |
| Putamen right R2* | 18.78 (18.13–19.39) | 19.86 (19.23–20.56) | 0.000 | 19.24 (17.66–20.63) | 20.13 (19.48–22.38) | 0.025 | 0.355 | 0.198 |
| Thalamus left R2* | 16.78 (16–17.39) | 17.93 (17.18–18.21) | 0.001 | 17.13 (16.2–18.94) | 19.38 (18.4–20.1) | 0.001 | 0.176 | <0.000 |
| Thalamus right R2* | 16.9412 (16.43–17.54) | 18.08 (17.43–18.73) | 0.001 | 17.37 (16.07–18.62) | 18.92 (17.9–19.87) | 0.005 | 0.597 | 0.060 |

| Subjects Included in the Gut Metagenome Analysis | Control Group (n = 14) | | | Subjects With Obesity (n = 13) | | | | |
|---|---|---|---|---|---|---|---|---|
| | Baseline | Follow-Up | | Baseline | Follow-Up | | Baseline | Follow-Up |
| | Median (Q1–Q3) | Median (Q1–Q3) | *P* Value | Median (Q1–Q3) | Median (Q1–Q3) | *P* Value | *P* Value | *P* Value |
| Age, y | 54 (40–58) | 42.5 (57–60.5) | <0.000 | 53.5 (48–58) | 56.5 (50.75–60.25) | 0.001 | 0.770 | 0.771 |
| Sex, female frequency | 6 (—) | – (—) | — | 9 (—) | – (—) | — | 0.573 | |
| Waist circumference, cm | 83 (73.5–92) | 91.5 (76–103) | 0.007 | 128.5 (122.5–135) | 128.5 (103–138) | 0.838 | <0.000 | 0.001 |
| BMI, kg/m$^2$ | 23.2 (21.4–25.65) | 23.8 (21.35–26.3) | 0.108 | 46.15 (39.35–48.02) | 38.85 (33.35–45.32) | 0.209 | <0.000 | <0.000 |
| Acidobacteria | 0.018 (0.012–0.026) | 0.013 (0.01–0.02) | 0.249 | 0.014 (0.007–0.021) | 0.014 (0.007–0.025) | 0.470 | 0.133 | 0.627 |
| Actinobacteria | 6.236 (4.943–8.718) | 10.37 (4.27–11.52) | 0.087 | 6.503 (3.352–11.763) | 7.373 (4.568–9.003) | 0.975 | 1.000 | 0.467 |
| Aquificae | 0.006 (0.005–0.008) | 0.004 (0.003–0.006) | 0.016 | 0.005 (0.004–0.006) | 0.005 (0.003–0.006) | 0.470 | 0.089 | 0.627 |
| Armatimonadetes | 0 (0–0.001) | 0.001 (0–0.001) | 0.600 | 0 (0–0.001) | 0 (0–0.001) | 0.221 | 0.409 | 0.734 |
| Bacteroidetes | 19.05 (16.3–35.52) | 28.9 (26.38–37.02) | 0.116 | 20.07 (12.2–23.98) | 22.28 (16.33–31.26) | 0.433 | 0.382 | 0.052 |
| Caldiserica | 0 (0–0.001) | 0 (0–0.001) | 0.753 | 0 (0–0) | 0 (0–0) | 0.730 | 0.660 | 0.052 |
| Candidatus Saccharibacteria | 0.001 (0.001–0.001) | 0.001 (0–0.001) | 0.600 | 0.001 (0.001–0.002) | 0.001 (0–0.002) | 0.124 | 0.544 | 0.884 |
| Chlamydiae | 0.001 (0.001–0.002) | 0.001 (0.001–0.002) | 0.422 | 0.001 (0.001–0.002) | 0.001 (0.001–0.002) | 0.363 | 0.225 | 0.771 |
| Chlorobi | 0.01 (0.008–0.014) | 0.008 (0.006–0.012) | 0.116 | 0.009 (0.005–0.012) | 0.009 (0.005–0.016) | 0.096 | 0.133 | 0.593 |
| Chloroflexi | 0.029 (0.023–0.045) | 0.026 (0.021–0.035) | 0.279 | 0.028 (0.021–0.034) | 0.024 (0.013–0.038) | 0.875 | 0.244 | 0.808 |
| Chrysiogenetes | 0.002 (0–0.003) | 0.001 (0.001–0.002) | 0.422 | 0.001 (0.001–0.002) | 0.001 (0.001–0.002) | 0.300 | 0.332 | 0.846 |
| Cloacimonetes | 0 (0–0.001) | 0 (0–0.001) | 0.311 | 0 (0–0.001) | 0 (0–0.001) | 0.534 | 0.527 | 0.961 |
| Cyanobacteria | 0.023 (0.02–0.029) | 0.02 (0.016–0.024) | 0.075 | 0.022 (0.015–0.026) | 0.019 (0.014–0.027) | 0.925 | 0.357 | 1.000 |
| Deferribacteres | 0.003 (0.003–0.005) | 0.003 (0.002–0.003) | 0.028 | 0.003 (0.002–0.004) | 0.003 (0.003–0.004) | 0.638 | 0.409 | 0.332 |

(*Continued*)

**Table 1. Continued**

| Subjects Included in the Gut Metagenome Analysis | Control Group (n = 14) | | | Subjects With Obesity (n = 13) | | | | |
|---|---|---|---|---|---|---|---|---|
| | Baseline | Follow-Up | | Baseline | Follow-Up | | Baseline | Follow-Up |
| | Median (Q1–Q3) | Median (Q1–Q3) | *P* Value | Median (Q1–Q3) | Median (Q1–Q3) | *P* Value | *P* Value | *P* Value |
| Deinococcus Thermus | 0.029 (0.023–0.045) | 0.023 (0.016–0.036) | 0.221 | 0.029 (0.016–0.035) | 0.024 (0.009–0.041) | 0.730 | 0.357 | 0.846 |
| Dictyoglomi | 0.002 (0.001–0.003) | 0.002 (0.001–0.002) | 0.422 | 0.002 (0.001–0.002) | 0.001 (0.001–0.003) | 0.245 | 0.244 | 0.808 |
| Elusimicrobia | 0.001 (0–0.001) | 0 (0–0.002) | 0.152 | 0.001 (0–0.001) | 0.001 (0–0.001) | 0.331 | 0.173 | 0.610 |
| Fibrobacteres | 0.009 (0.008–0.012) | 0.007 (0.005–0.01) | 0.019 | 0.009 (0.006–0.011) | 0.009 (0.004–0.012) | 0.975 | 0.771 | 0.528 |
| Firmicutes | 67.86 (51.86–73.47) | 55.47 (48.01–59.45) | 0.011 | 66.34 (54.42–73.55) | 64.64 (52.62–70.7) | 0.331 | 0.884 | 0.120 |
| Fusobacteria | 0.111 (0.096–0.134) | 0.082 (0.07–0.107) | 0.028 | 0.105 (0.085–0.11) | 0.1 (0.087–0.115) | 0.778 | 0.308 | 0.174 |
| Gemmatimonadetes | 0.001 (0.001–0.002) | 0.001 (0–0.001) | 0.173 | 0.001 (0–0.001) | 0.001 (0.001–0.002) | 0.084 | 0.089 | 0.244 |
| Ignavibacteriae | 0.003 (0.001–0.003) | 0.002 (0.001–0.002) | 0.019 | 0.002 (0.001–0.002) | 0.002 (0.001–0.003) | 0.198 | 0.042 | 0.627 |
| Nitrospirae | 0.003 (0.002–0.003) | 0.002 (0.001–0.003) | 0.046 | 0.002 (0.001–0.003) | 0.002 (0.001–0.003) | 0.826 | 0.109 | 0.560 |
| Planctomycetes | 0.011 (0.006–0.015) | 0.006 (0.005–0.009) | 0.152 | 0.007 (0.004–0.009) | 0.006 (0.004–0.013) | 0.551 | 0.081 | 0.961 |
| Proteobacteria | 2.759 (2.539–3.605) | 2.989 (2.399–3.606) | 0.753 | 2.936 (2.055–3.511) | 3.072 (2.004–8.225) | 0.397 | 0.884 | 0.593 |
| Spirochetes | 0.186 (0.156–0.27) | 0.171 (0.147–0.184) | 0.116 | 0.161 (0.136–0.201) | 0.177 (0.123–0.203) | 0.551 | 0.099 | 0.771 |
| Synergistetes | 0.127 (0.093–0.239) | 0.102 (0.079–0.142) | 0.173 | 0.112 (0.064–0.139) | 0.119 (0.047–0.213) | 0.433 | 0.207 | 0.846 |
| Tenericutes | 0.035 (0.022–0.049) | 0.018 (0.016–0.059) | 0.463 | 0.025 (0.018–0.035) | 0.023 (0.018–0.028) | 0.551 | 0.109 | 0.771 |
| Thermodesulfobacteria | 0.001 (0–0.002) | 0.001 (0–0.001) | 0.422 | 0 (0–0.001) | 0.001 (0–0.001) | 0.594 | 0.073 | 0.771 |
| Thermotoga | 0.009 (0.007–0.014) | 0.007 (0.006–0.01) | 0.116 | 0.009 (0.007–0.01) | 0.01 (0.006–0.01) | 0.778 | 0.438 | 0.332 |
| Verrucomicrobia | 0.03 (0.016–0.056) | 0.03 (0.009–0.418) | 0.972 | 0.021 (0.008–0.107) | 0.037 (0.015–0.103) | 0.826 | 0.560 | 0.734 |

Qualitative variables are expressed as frequencies and quantitative variables are expressed as median (Q1–Q3). Nonparametric Wilcoxon test was used to assess intrasubject differences at baseline and follow-up. The Mann-Whitney *U* test was used to state the differences between subjects with obesity and control group at baseline and follow-up. R2* rates are expressed in Hz and microbiome abundance values are given in %.

Abbreviations: HDL, high-density lipoprotein; LDL, low-density lipoprotein.

phonemic verbal (but not semantic) fluency score at follow-up [Fig. 4(b)].

Remarkably, Fig. 5 shows the brain areas linked to the percent change in Tenericutes RA over the 2-year period. Those subjects with an increase in Tenericutes had significantly less R2* increase in those areas highlighted in Fig. 5, notably the striatum ($P < 0.0001$), in parallel to spared visual-spatial constructional ability (Fig. 2). In

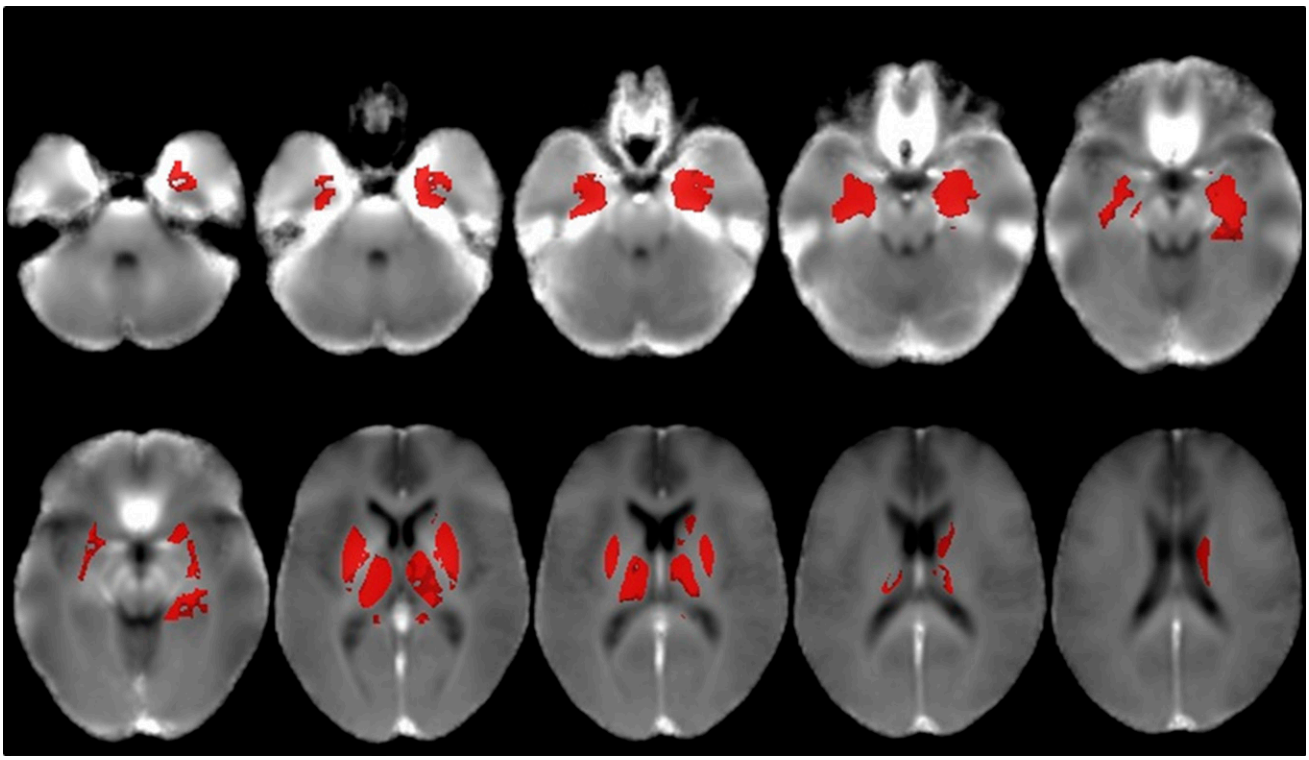

**Figure 1.** Statistical mapping of the brain nuclei showing those areas with increased R2* in the voxelwise analysis (5000 iterations). The significant increase in the relaxation rates in a specific area is highlighted in red ($P < 0.0001$).

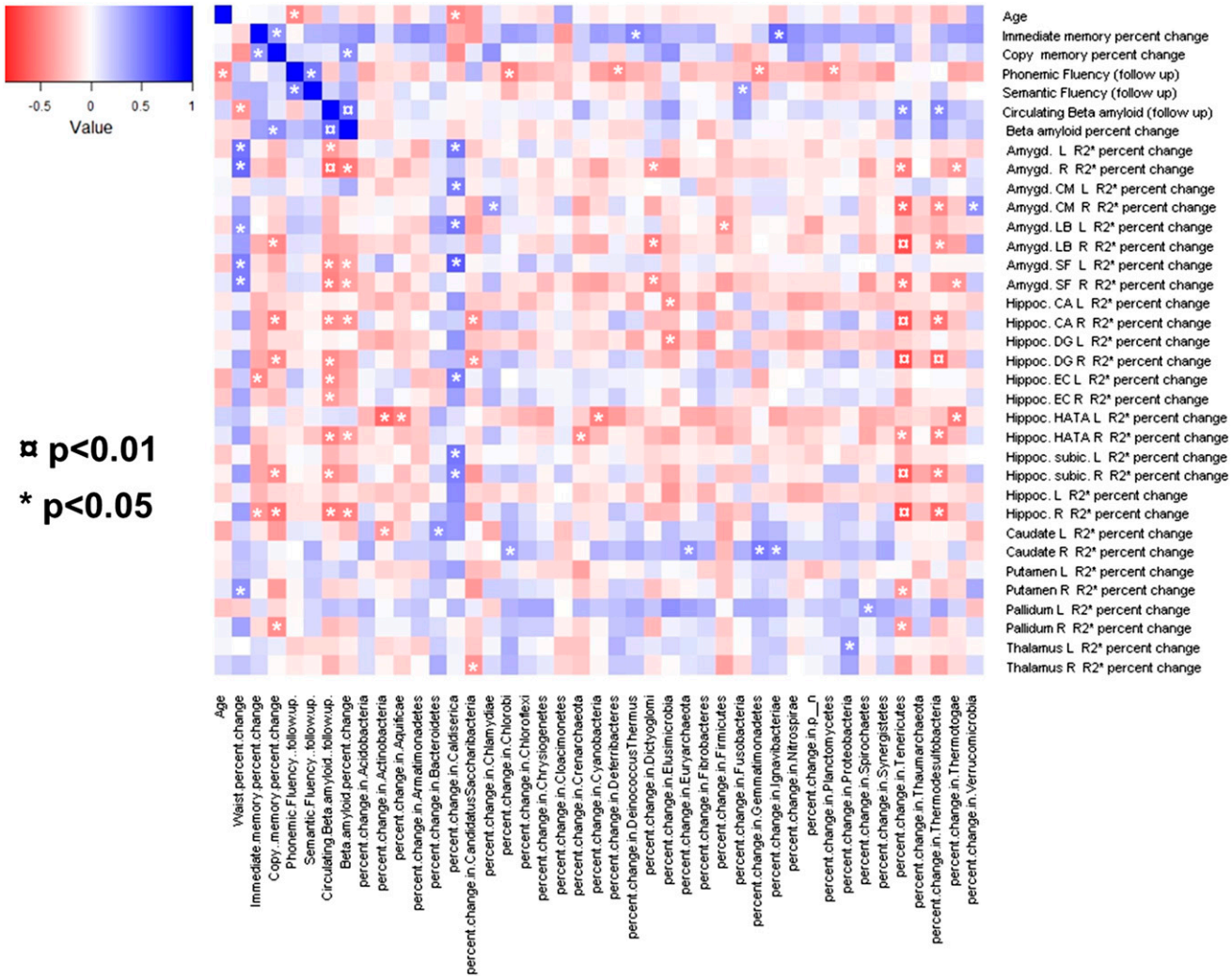


**Figure 2.** Heat map of the associations among metabolic, cognitive, brain structure variables, and gut microbiota composition at the phylum level. The Hheat map shows the correlation coefficients (Spearman analysis) between variables, where the intensity of the color (positive [blue] or negative [red]) is proportional to the strength of the association. $*P < 0.05$, $¤P < 0.01$.

addition, the percent increase in Tenericutes RA was associated with better scores in TMT-B after excluding those subjects who gained weight. This score is indicative of better working memory and inhibition of automatic responses, both being aspects of cognition controlled by the striatum (15). The highest increase in Tenericutes RA was also associated positively with circulating A$\beta$42 at follow-up (Supplemental Table 1), suggesting protection from cognitive worsening with increased RA. The increase in Thermodesulfobacteria RA was also independently and positively associated with A$\beta$42 at follow-up ($P = 0.008$).

Regarding the metagenome, we focused on those functions significantly associated with systemic iron stores (measured as serum ferritin concentration) at both baseline and follow-up. The values of the selected functions were similar in men and women, so all subjects were evaluated as a whole. Interestingly, the functions associated with serum ferritin were also associated with brain iron levels in the striatum at baseline and at follow-up (Supplemental Fig. 1). Of note, the change in iron content in specific areas of the striatum was associated with the change in functional genomes, specifically in obese subjects (Supplemental Fig. 1). Of these functions, pyridoxal phosphate, phosphoenolpyruvate, and acetyl-coenzyme A carboxylase have been described to be affected by iron (23–26).

## Discussion

There is increasing evidence of the contribution of enteric microbiota to the gut-brain axis in animal models. In humans, there is little evidence of its existence, and the study of this signaling pathway is in its infancy (9, 10). Although brain structure (changes in iron content) in normal subjects is known to change within a 2-year period (12), this study explores the effects of weight loss.

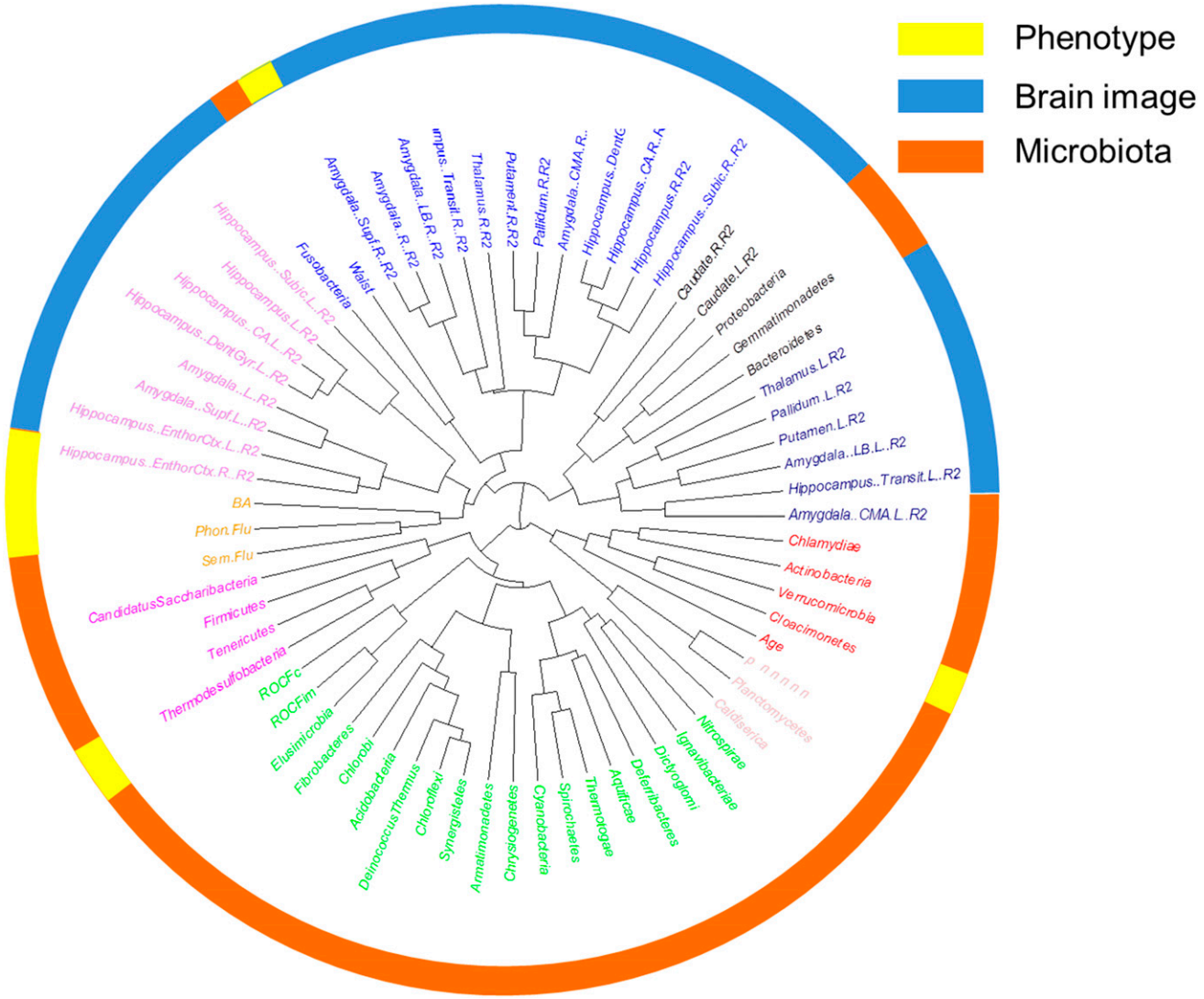


**Figure 3.** Clustering analyses reveal that 2-year changes in microbiota aggregate with changes in R2* values at specific nuclei and phenotype variations. After scaling these variables and calculating Euclidean distances using the R package dist, these variables were clusterized using a complete type algorithm. By using the *clustsig* R package, nine clusters appeared ($P < 0.0001$ over nonclustering). The cladogram shows the obtained hierarchical clustering with related variables appearing closer. This clustering aggregated several age-related changes in phenotype, microbiota, and biochemistry together. As an example, 2-year changes in verbal and semantic fluency was more associated with variations in A$\beta$42 than with changes in other variables; 2-year alterations in waist clustered with variations in Fusobacteria; and changes in the abundance of several bacterial phyla were linked to shifts in neuroimaging R2* values, suggesting a biological association between these variations. Outer circle indicates type of variable clustered.

Given that obese subjects exhibited increased brain iron content linked to cognitive dysfunction (14), we anticipated an improvement of iron deposition with diet-induced weight loss. This was not the case after a 2-year period. The increase in R2* was observed in the same proportion in subjects that gained or lost BMI, suggesting that total body mass was not the most important factor influencing the percent increase in R2*. However, this finding also suggests that there is a time effect that seems to be independent of obesity. In the search of factors that could influence R2* increase, we found that shifts in gut microbiota were linked to longitudinal changes in brain structure and function.

Shifts in Gemmatimonadetes, Bacteroidetes and Proteobacteria, Caldiserica, Candidatus Saccharibacteria, Tenericutes, Thermodesulfobacteria, and Chlorobi RA were associated with increased percent change of R2* at the striatum, superficial amygdala and hippocampus [Fig. 4(a)]. In this last territory, the phyla Fibrobacteres, Synergistetes, and Tenericutes RA were reciprocally associated with right hippocampus R2*.

The increase in Tenericutes RA was also associated positively with circulating A$\beta$42 at follow-up and less R2* increase. This is potentially important because the increase in circulating $\beta$-amyloid A$\beta$42 levels was positively associated with the change in visual-spatial

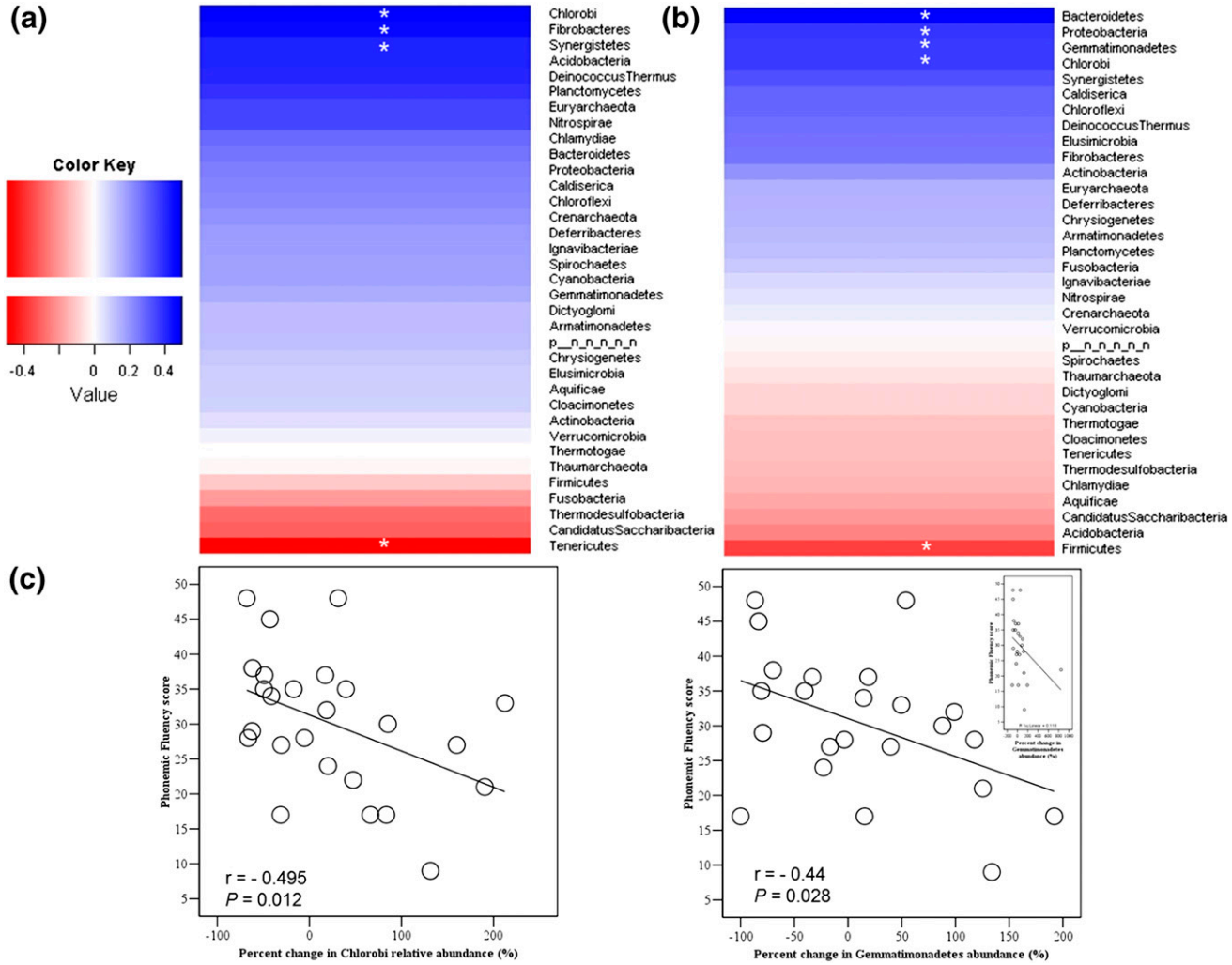


**Figure 4.** Multivariate analyses of the associations among variations changes in microbiota and R2* values at hippocampus, amygdala, and caudate nucleus. Heat maps showing the multivariate analysis between changes in gut microbiota and brain nuclei R2* after adjusting for age, sex, and/or waist circumference. *Statistically significant associations, with $P < 0.05$. (a) Regression models adjusting for age and waist change variation showing the positive association between R2* changes at the right hippocampus with changes in Chlorobi, Fibrobacteres, and Synergistetes and negatively with Tenericutes. (b) Regression models adjusting for age and sex showing the significant associations ($P < 0.05$) between right caudate nucleus R2* variations and Bacteroidetes, Proteobacteria, Gemmatimonadetes, Chlorobi (positive association), and Firmicutes (inverse association). (c) Linear regression analyses showing the negative association between phonemic fluency scores and the percent change in Chlorobi and Gemmatimonadetes. Note that two subjects without Chlorobi and Gemmatimonadetes detection at follow-up were excluded from the analyses.

constructional ability and immediate memory and negatively with the increase in R2*. A decrease in A$\beta$42 levels are thought to reflect compartmentalization of A$\beta$ peptides in the brain and have been related to the development of Alzheimer's disease (22). In line with these associations, there is previous evidence that Tenericutes are able to efficiently and rapidly degrade $\beta$-amyloid (27). This could happen within the gut, where $\beta$-amyloid has been detected, resulting in relatively higher circulating A$\beta$42 levels (28). In fact, neuroprotective effects of *Mycoplasma hyorhinis* against amyloid-$\beta$-peptide toxicity have been demonstrated in human neuroblastoma cells (29).

The reasons for the apparent protective associations of Tenericutes and Thermodesulfobacteria are unclear, but one interesting speculation is that it could be mediated through metabolization of arsenic, an agent that has been implicated in the pathophysiology of Alzheimer's disease in epidemiological studies (30, 31). Both Thermodesulfobacteria (32) and Tenericutes (33) are able to actively metabolize arsenic, decreasing its impact on the aging brain.

The ability to capture iron is a challenge for most bacteria. Interestingly, several of the functions associated with body iron stores are involved in the generation of siderophores in bacteria (phospho-2-dehydro-3-deoxyheptonate aldolases (34) and phosphoenolpyruvate (35)). Also of note, the function gluconate was not only associated with serum ferritin at baseline and at follow-up, but also with iron content in the left caudate nucleus at baseline, with R2* at the left putamen nucleus at follow-up, whereas the percent change in this function was also positively

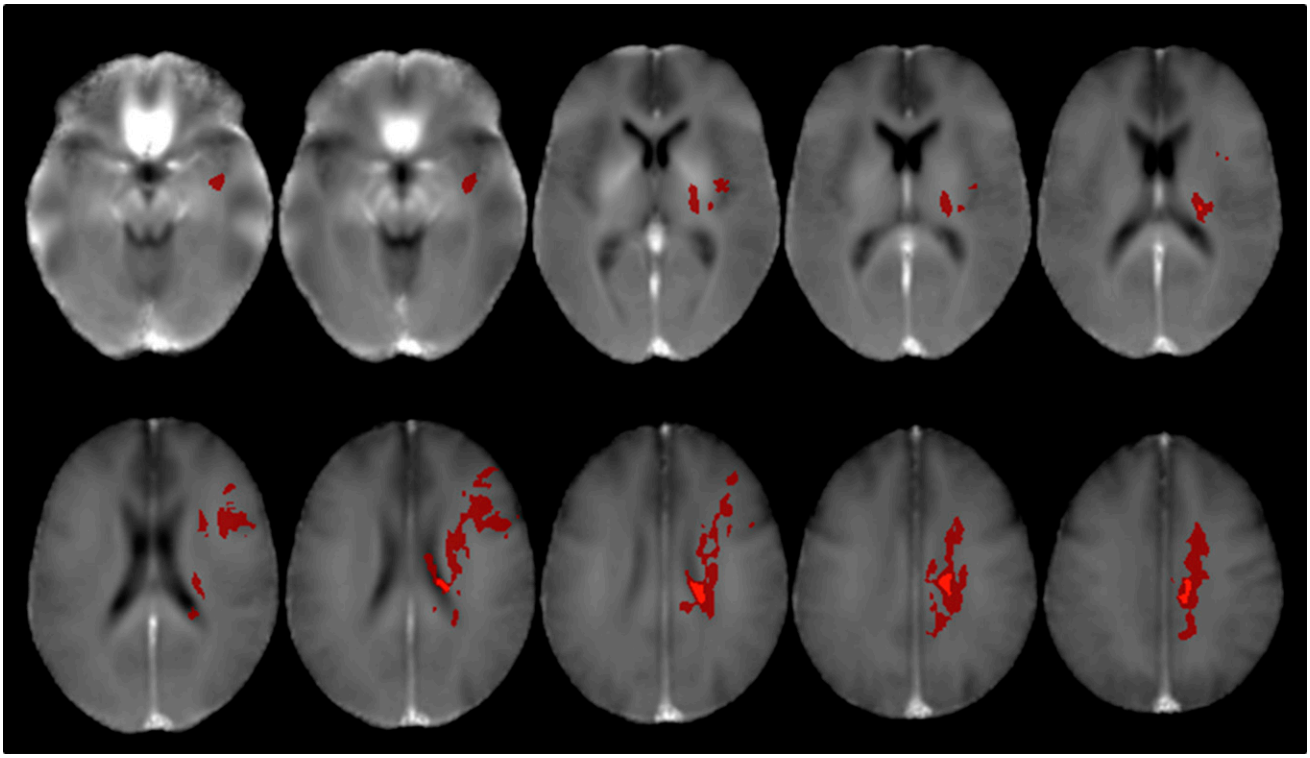

**Figure 5.** Statistical mapping of the increasing R2* differences according to the increase in Tenericutes. The images highlight in red those regions where the R2* increase was more attenuated in those subjects with the highest increase in Tenericutes in the voxelwise analysis after 5000 iterations ($P < 0.0001$).

associated with percent R2* increase at this last nucleus. Extracellular gluconate has been described to promote dissolution of Fe minerals (36). There is a large increase in gluconate secretion from bacteria with changing iron in the environment (36). Some specific phyla were associated with systemic and tissue markers of iron in parallel to decreased immediate and visual-spatial constructional ability. These findings are in line with brain iron deposition linked to cognitive status in middle-aged subjects (14).

In concordance with other studies we found the RA of Prevotellaceae positively correlated with BMI, whereas the RA of Bacteroidaceae, Rikenellaceae, and Lachnospiraceae was negatively associated (37).

In summary, changes in brain iron and cognitive function run in parallel to specific bacterial phyla of the gut microbiota. Considering that gut microbiota has been linked to other human pathologies that are centrally controlled, such as schizophrenia (38), autism and mood disorders (39), as well as obesity (40), it will be interesting to further explore the molecular and cellular mechanism by which gut bacteria might influence these relationships.

## Acknowledgments

Address all correspondence to: J. M. Fernandez-Real, MD, PhD, Section of Diabetes, Endocrinology and Nutrition, Hospital of Girona "Dr Josep Trueta," Carretera de França s/n, 17007 Girona, Spain. E-mail: jmfreal@idibgi.org.

This study was supported by Instituto de Salud Carlos III (PI 14/1115 and PI 15/01934), Ministry of Economy and Competitiveness (SAF2015-65878-R), and PROMETEO II/2014/065 (Generalitat Valenciana). CIBER de la Fisiopatología de la Obesidad y la Nutrición is an initiative of the Instituto de Salud Carlos III. This study was also supported by Fondo Europeo de Desarrollo Regional and European Community's Seventh Framework Programme (FP7/2007-2013) under Grant Agreement 281854 "the ObERStress project" (M.L.).

Disclosure Summary: The authors declare no conflicts of interest in this work.

## References

1. Rhee SH, Pothoulakis C, Mayer EA. Principles and clinical implications of the brain-gut-enteric microbiota axis. *Nat Rev Gastroenterol Hepatol*. 2009;**6**(5):306–314.
2. Mayer EA, Tillisch K, Gupta A. Gut/brain axis and the microbiota. *J Clin Invest*. 2015;**125**(3):926–938.
3. Hartstra AV, Bouter KE, Bäckhed F, Nieuwdorp M. Insights into the role of the microbiome in obesity and type 2 diabetes. *Diabetes Care*. 2015;**38**(1):159–165.
4. Turnbaugh PJ, Hamady M, Yatsunenko T, Cantarel BL, Duncan A, Ley RE, Sogin ML, Jones WJ, Roe BA, Affourtit JP, Egholm M, Henrissat B, Heath AC, Knight R, Gordon JI. A core gut microbiome in obese and lean twins. *Nature*. 2009;**457**(7228):480–484.
5. Sweeney TE, Morton JM. The human gut microbiome: a review of the effect of obesity and surgically induced weight loss. *JAMA Surg*. 2013;**148**(6):563–569.

6. Ley RE, Turnbaugh PJ, Klein S, Gordon JI. Microbial ecology: human gut microbes associated with obesity. *Nature*. 2006;**444**(7122): 1022–1023.
7. Menni C, Jackson MA, Pallister T. Gut microbiome diversity and high fibre intake are related to lower long term weight gain [published online ahead of print April 4, 2017]. *Int J Obes*. doi: 10.1038/ijo.2017.66.
8. Dinan TG, Stilling RM, Stanton C, Cryan JF. Collective unconscious: how gut microbes shape human behavior. *J Psychiatr Res*. 2015;**63**:1–9.
9. Fernández-Real JM, Serino M, Blasco G, Puig J, Daunis-i-Estadella J, Ricart W, Burcelin R, Fernández-Aranda F, Portero-Otin M. Gut microbiota interacts with brain microstructure and function. *J Clin Endocrinol Metab*. 2015;**100**(12):4505–4513.
10. Tillisch K, Labus J, Kilpatrick L, Jiang Z, Stains J, Ebrat B, Guyonnet D, Legrain-Raspaud S, Trotin B, Naliboff B, Mayer EA. Consumption of fermented milk product with probiotic modulates brain activity. *Gastroenterology*. 2013;**144**(7):1394–1401, 1401. e1–1401.e4.
11. Haacke EM, Cheng NY, House MJ, Liu Q, Neelavalli J, Ogg RJ, Khan A, Ayaz M, Kirsch W, Obenaus A. Imaging iron stores in the brain using magnetic resonance imaging. *Magn Reson Imaging*. 2005;**23**(1):1–25.
12. Daugherty AM, Haacke EM, Raz N. Striatal iron content predicts its shrinkage and changes in verbal working memory after two years in healthy adults. *J Neurosci*. 2015;**35**(17):6731–6743.
13. Schröder N, Figueiredo LS, de Lima MN. Role of brain iron accumulation in cognitive dysfunction: evidence from animal models and human studies. *J Alzheimers Dis*. 2013;**34**(4):797–812.
14. Blasco G, Puig J, Daunis-I-Estadella J, Molina X, Xifra G, Fernández-Aranda F, Pedraza S, Ricart W, Portero-Otín M, Fernández-Real JM. Brain iron overload, insulin resistance, and cognitive performance in obese subjects: a preliminary MRI case-control study. *Diabetes Care*. 2014;**37**(11):3076–3083.
15. Herrero MT, Barcia C, Navarro JM. Functional anatomy of thalamus and basal ganglia. *Childs Nerv Syst*. 2002;**18**(8): 386–404.
16. Meadowcroft MD, Peters DG, Dewal RP, Connor JR, Yang QX. The effect of iron in MRI and transverse relaxation of amyloid-beta plaques in Alzheimer's disease. *NMR Biomed*. 2015;**28**(3): 297–305.
17. Wood JC, Enriquez C, Ghugre N, Tyzka JM, Carson S, Nelson MD, Coates TD. MRI R2 and R2* mapping accurately estimates hepatic iron concentration in transfusion-dependent thalassemia and sickle cell disease patients. *Blood*. 2005;**106**(4):1460–1465.
18. Alústiza JM, Artetxe J, Castiella A, Agirre C, Emparanza JI, Otazua P, García-Bengoechea M, Barrio J, Mújica F, Recondo JA; Gipuzkoa Hepatic Iron Concentration by MRI Study Group. MR quantification of hepatic iron concentration. *Radiology*. 2004; **230**(2):479–484.
19. Daugherty A, Raz N. Age-related differences in iron content of subcortical nuclei observed in vivo: a meta-analysis. *Neuroimage*. 2013;**70**:113–121.
20. Schmieder R, Edwards R. Quality control and preprocessing of metagenomic datasets. *Bioinformatics*. 2011;**27**(6):863–864.
21. Langmead B, Salzberg SL. Fast gapped-read alignment with Bowtie 2. *Nat Methods*. 2012;**9**(4):357–359.
22. Schupf N, Tang MX, Fukuyama H, Manly J, Andrews H, Mehta P, Ravetch J, Mayeux R. Peripheral Abeta subspecies as risk biomarkers of Alzheimer's disease. *Proc Natl Acad Sci USA*. 2008; **105**(37):14052–14057.
23. Zhang J, Lewis RM, Wang C, Hales N, Byrne CD. Maternal dietary iron restriction modulates hepatic lipid metabolism in the fetuses. *Am J Physiol Regul Integr Comp Physiol*. 2005;**288**(1): R104–R111.
24. Plank DW, Gengenbach BG, Gronwald JW. Effect of iron on activity of soybean multi-subunit acetyl-coenzyme A carboxylase. *Physiol Plant*. 2001;**112**(2):183–194.
25. Lee HJ, Choi JS, Lee HJ, Kim WH, Park SI, Song J. Effect of excess iron on oxidative stress and gluconeogenesis through hepcidin during mitochondrial dysfunction. *J Nutr Biochem*. 2015;**26**(12): 1414–1423.
26. Kyaw A, Nwe KK, Pe UH. Decreased pyridoxal phosphate and kinase levels in iron-deficient rat liver. *Biochem Med*. 1980;**23**(1): 17–24.
27. Zhao H, Dreses-Werringloer U, Davies P, Marambaud P. Amyloid-beta peptide degradation in cell cultures by mycoplasma contaminants. *BMC Res Notes*. 2008;**1**:38.
28. Cabal A, Alonso-Cortina V, Gonzalez-Vazquez LO, Naves FJ, Del Valle ME, Vega JA. beta-Amyloid precursor protein (beta APP) in human gut with special reference to the enteric nervous system. *Brain Res Bull*. 1995;**38**(5):417–423.
29. Elkind E, Vaisid T, Kornspan JD, Barnoy S, Rottem S, Kosower NS. Neuroprotective effects of Mycoplasma hyorhinis against amyloid-β-peptide toxicity in SH-SY5Y human neuroblastoma cells are mediated by calpastatin upregulation in the mycoplasma-infected cells. *Neurochem Int*. 2011;**58**(4):497–503.
30. Edwards M, Johnson L, Mauer C, Barber R, Hall J, O'Bryant S. Regional specific groundwater arsenic levels and neuropsychological functioning: a cross-sectional study. *Int J Environ Health Res*. 2014;**24**(6):546–557.
31. Chin-Chan M, Navarro-Yepes J, Quintanilla-Vega B. Environmental pollutants as risk factors for neurodegenerative disorders: Alzheimer and Parkinson diseases. *Front Cell Neurosci*. 2015;**9**:124.
32. Hamamura N, Macur RE, Korf S, Ackerman G, Taylor WP, Kozubal M, Reysenbach AL, Inskeep WP. Linking microbial oxidation of arsenic with detection and phylogenetic analysis of arsenite oxidase genes in diverse geothermal environments. *Environ Microbiol*. 2009;**11**(2):421–431.
33. Luo J, Bai Y, Liang J, Qu J. Metagenomic approach reveals variation of microbes with arsenic and antimony metabolism genes from highly contaminated soil. *PLoS One*. 2014;**9**(10):e108185.
34. Lemaître C, Bidet P, Benoist JF, Schlemmer D, Sobral E, d'Humières C, Bonacorsi S. The ssbL gene harbored by the ColV plasmid of an Escherichia coli neonatal meningitis strain is an auxiliary virulence factor boosting the production of siderophores through the shikimate pathway. *J Bacteriol*. 2014;**196**(7):1343–1349.
35. Hider RC, Kong X. Chemistry and biology of siderophores. *Nat Prod Rep*. 2010;**27**(5):637–657.
36. Sasnow SS, Wei H, Aristilde L. Bypasses in intracellular glucose metabolism in iron-limited Pseudomonas putida. *MicrobiologyOpen*. 2016;**5**(1):3–20.
37. Clarke SF, Murphy EF, Nilaweera K, Ross PR, Shanahan F, O'Toole PW, Cotter PD. The gut microbiota and its relationship to diet and obesity: new insights. *Gut Microbes*. 2012;**3**(3):186–202.
38. Dinan TG, Borre YE, Cryan JF. Genomics of schizophrenia: time to consider the gut microbiome? *Mol Psychiatry*. 2014;**19**(12): 1252–1257.
39. Mangiola F, Ianiro G, Franceschi F, Fagiuoli S, Gasbarrini G, Gasbarrini A. Gut microbiota in autism and mood disorders. *World J Gastroenterol*. 2016;**22**(1):361–368.
40. Schéle E, Grahnemo L, Anesten F, Hallén A, Bäckhed F, Jansson JO. The gut microbiota reduces leptin sensitivity and the expression of the obesity-suppressing neuropeptides proglucagon (Gcg) and brain-derived neurotrophic factor (Bdnf) in the central nervous system. *Endocrinology*. 2013;**154**(10):3643–3651.